Chapter 3
The Potential Application of Biochars for Dyes with an Emphasis on Azo Dyes: Analysis Through an Experimental Case Study Utilizing Fruit-Derived Biochar for the Abatement of Congo Red as the Model Pollutant

Kumar Vikrant, Kangkan Roy, Mandavi Goswami, Himanshu Tiwari, Balendu Shekher Giri, Ki-Hyun Kim, Yui Fai Tsang, and Ram Sharan Singh

Abstract The unbridled industrialization and unrestrained expansion of modern textile facilities combined with a deficiency of adequate treatment provisions have escalated the discharge of toxic effluents rich in carcinogenic pollutants such as dyes. As a consequence, there is an alarming need for the development of financially suitable and highly efficient treatment options to protect the immaculate ecosystems, natural resources, and human health. In this respect, adsorption-based treatment options have attracted widespread attention as eco-friendly and cost-

Authors Kumar Vikrant and Kangkan Roy have been contributed equally to this chapter.

K. Vikrant
Department of Chemical Engineering and Technology, Indian Institute of Technology, Banaras Hindu University, Varanasi, India

Department of Civil and Environmental Engineering, Hanyang University, Seoul, Republic of Korea

K. Roy · H. Tiwari · B. S. Giri (✉) · R. S. Singh
Department of Chemical Engineering and Technology, Centre of Advanced Study, Indian Institute of Technology, Banaras Hindu University, Varanasi, India

M. Goswami
Department of Bioengineering, Integral University, Lucknow, Uttar Pradesh, India

K.-H. Kim (✉)
Department of Civil and Environmental Engineering, Hanyang University, Seoul, Republic of Korea
e-mail: kkim61@hanyang.ac.kr

Y. F. Tsang
Department of Science and Environmental Studies, The Education University of Hong Kong, Tai Po, New Territories, Hong Kong, China

effective approach. Biochar has propelled itself to the forefront of the scientific community as a highly economical sorbent with great adsorption capabilities. Notably, biochars provide a win-win strategy by simultaneously utilizing the waste biomass during its production and a great adsorbent for pollutant removal. Although biochars have been applied for the treatment of various dyes, there have been very few reports of its application for Congo red (CR) dye. In this book chapter we analyze the application of biochar for dyes with particular focus on CR. We try to practically understand the mechanism of interaction between biochar and CR molecules (a model anionic azo dye) by elucidating an experimental case study. The case study will provide valuable insights into the importance of the utilization of locally available bio waste for economic biochar production and the mechanism of removal of anionic dyes through biochars. In brief, the adsorptive removal of CR was investigated using Arjun fruit biochar (AFB) derived from the fruit of locally grown *Terminalia arjuna*. The sorptive removal of CR on AFB was investigated under the following operational conditions (pH, 2–12; biochar dosage, 4–14 g/L; temperature, 30–60 °C; and contact time, 30–480 min). The sorption behavior of CR was well described through the Langmuir monolayer model ($R^2 = 0.9985$) and pseudo-second order kinetics ($R^2 \geq 0.9977$) for all tested CR levels (20–100 mg/L). The results of thermodynamic analysis revealed that the sorption of CR onto AFB proceeded favorably and spontaneously.

Keywords Adsorption · *Terminalia arjuna* · Dye · Biochar · Kinetics · Thermodynamics

3.1 Introduction

Recent years have witnessed prolific rise in endeavors focused towards water quality management due to the ever rising issues concerned with water pollution (Mekonnen Mesfin and Hoekstra Arjen 2017; D'Inverno et al. 2018). The regulation and removal of baleful water pollutants such as dyes have been recognized as prime task by environmental bodies such as the United States Environmental Protection Agency (US EPA) (Vikrant et al. 2018). Hence, extensive investigations have been undertaken to analyze the long as well as short term effects of dyes on ecosystems and human health (Chung 2016).

Dyes are chemical compounds with intense color and extremely high water solubility. A wide variety of dyes and pigments are utilized in paper, textile, paint, drugs, tanning, food, and cosmetic industries (Chen et al. 2018; Vikrant et al. 2018). The ubiquitous presence of highly toxic synthetic dye compounds in water bodies poses grave health concerns as these chemicals are known to be highly carcinogenic and mutagenic (Abu Talha et al. 2018). Dyes impart intense color to water, making it

aesthetically displeasing. They also cause an imbalance in the aquatic ecosystems by increasing chemical oxygen demand and lowering light penetration (Vikrant et al. 2018). Also, very low removal rate is generally observed for dyes during secondary and primary wastewater treatment owing to their recalcitrant structures resulting in there swift carryover into water bodies (Meerbergen et al. 2018). As a consequence, toxic dye molecules bioaccumulate in the ecosystem and get transmitted to the potable water supply (Leo et al. 2018). Microbial mediated services are also considered as valuable means for water treatments and restoration of degraded ecosystems (Singh et al. 2017a, b; Vimal et al. 2018; Kumar et al. 2018; Singh 2019; Singh and Singh 2019; Singh et al. 2019a,b; Vimal and Singh 2019).

Azo dyes are the most common variety of dyes in used today and is the oldest industrially synthesized compound (Vikrant et al. 2018). Interestingly, azo dyes comprise around 60% of the total dyes being used in the textile industry, thus posing a significant threat (Munagapati and Kim 2016). Azo dyes attract widespread usage in various industries owing to their multiple advantages such as easy usage, wide availability of color range, great photostability, low requirement of energy, and great covalent adherence with textiles (Brüschweiler and Merlot 2017). The chromophoric -N=N- groups in nonionic and anionic dyes undergoes reductive breakage to result in the formation of highly virulent aromatic amines (Jayapal et al. 2018). Congo red (CR) is a major azo dye utilized extensively in the cellulose industries (e.g., pulp, paper, and cotton textiles) (Chen et al. 2018). The recalcitrant and toxic nature of CR makes its removal from water bodies decidedly imperative (Vikrant et al. 2018).

Due to a synthetic origin and complex structure, the highly recalcitrant tendency of azo dyes renders them exceptionally stable towards heat and light. As such, their removal *via* conventional treatment techniques is not simple (Vikrant et al. 2018). A wide array of methodologies (e.g., photocatalysis (Zhao et al. 2018), ozone treatment (Mella et al. 2018), ultrasound treatment, oxidation (Nidheesh et al. 2018), coagulation-flocculation (Mella et al. 2018), application of membranes (Peydayesh et al. 2018), and biological processes (Vikrant et al. 2018) have been applied for the abatement of pigments and dyes from water/wastewater. Nevertheless, all these techniques suffer from environmental and economic shortcomings in terms of excessive operating and capital financial requirement, excessive sludge generation, and complex operational procedures (Munagapati and Kim 2016). Adsorption has been considered as an environmentally benign and economically advantageous alternative for the abatement of pigments/dyes from aqueous solutions (Chen et al. 2018; Vikrant et al. 2018). Adsorption is favored primarily because of the costs involved in the preparation and procurement of adsorbents and their regeneration (Vikrant et al. 2018). In recent years microbial services has been proposed as potential tool as bioremediation and restoration of polluted soil and environment (Singh 2013, 2014, 2015, 2016; Singh Boudh 2016; Kumar et al. 2017; Kumar and Singh 2017; Tiwari and Singh 2017).

3.2 Biochar for the Removal of Dyes

Sorptive removal of dyes has attracted extensive interest from the scientific community owing to its easy operation, environmental benignity, cost-effectiveness, and great selectivity (Pham et al. 2017; Pham et al. 2018; Sophia and Lima 2018). Selection of a suitable adsorbent both in terms of cost and efficiency is paramount towards designing a sorption-based dye treatment system. At present, pristine and carbonaceous adsorbents are extracted from various agricultural/biological wastes such as coconut shell (Bello and Ahmad 2012), rice husk (Singh and Srivastava 2001), rice straws (El-Sonbati et al. 2016), almond shell (Doulati Ardejani et al. 2008), and wood char (Bangash Fazlullah and Manaf 2013) for the abatement of organic wastes from water/wastewater. In recent years, biochar (a solid carbonaceous substance synthesized through the pyrolysis of biomass under conditions of low oxygen) has attracted widespread scientific attention as a novel tool for the abatement of aqueous contaminants owing to its large surface area, stable carbon matrix, and high porosity (Thines et al. 2017; Vikrant et al. 2018). Biochars provide a win-win strategy as they utilize potentially unwanted biomass (e.g., agricultural waste) and provide excellent sorptive media for toxic pollutant removal (Vikrant et al. 2018).

The *Terminalia arjuna* belongs to the family of Combretaceae and is indigenous to the Indian subcontinent (Amalraj and Gopi 2017). Its bark decoction has been traditionally utilized for curing numerous disorders related to the cardiovascular system such as dyslipidemia, angina, hypertension, and congestive heart failure (Dwivedi and Chopra 2014; Amalraj and Gopi 2017). Moreover, the crude drug made from the bark of *T. arjuna* possesses antioxidant, hypolipidemic, anti-ischemic, and anti-atherogenic activities (Dwivedi and Chopra 2014). However, the fruit of *T. arjuna* remains unused in the pharmaceutical industry (Amalraj and Gopi 2017).

In the presented experimental case study, Arjun fruit biochar (AFB) was synthesized from the fruit of *T. arjuna* and used as an adsorbent. The aim of the present investigation was to determine the feasibility of AFB as a sorbent for the abatement of CR from water. The effects of various operating parameters (e.g., pH of the solution, dose of biochar, contact time, initial concentration of CR, and temperature) on the adsorption behavior of CR and treatment performance were investigated. Kinetic, isothermal, and thermodynamic fits were utilized to understand the sorption phenomenon, underlying mechanisms, and equilibrium of the sorption process.

This case study was carried out to explore the possibility for a practical utilization of *T. arjuna* fruits which are commonly produced as waste biomass by the pharmaceutical industry (Amalraj and Gopi 2017). It is a known fact that the study site (i.e., Varanasi, India) has a dense cluster of local carpet industries that produce glut amounts of CR rich effluents (Abu Talha et al. 2018). In light of these environmental conditions, it was proposed that biochar should be produced from indigenous *T. arjuna* fruits and used subsequently in local dye remediation. Thus, based on this study, a practical solution was sought for the indigenous utilization of bio-

waste while at the same time pursuing a treatment for wastewater. Furthermore, the performance of the biochar was assessed at the original pH of the textile industry effluents. The results of this study were of enough relevance to showcase an economical and practical solution for the abatement of dye by biochar derived from biowaste. Such experimental studies clearly elucidate the practical application of biochar for CR removal.

3.3   Experimental Case Study – Materials and Methods

3.3.1   Preparation of Biochar

Arjun fruit were obtained from indigenous *T. arjuna* trees. A stainless-steel pyrolysis reactor (inside diameter, 75 mm; length, 1.10 m) was used for biochar production, in which the temperature was controlled by an electric heater. The Arjun fruit were cleansed with Milli-Q water and parched naturally for 10 days. The dried fruit were subsequently crushed followed by sieving (size of particles: 72 BSS mesh, i.e., 210 μm) and then 600 g of the fruit was pyrolyzed at 500 °C (heating rate: 5 °C/min) for 3 h. The pyrolyzed sample (i.e., biochar) was cleansed with hot Milli-Q water and then oven dried at 75 °C for 2 h (Oven Universal NSW-143). The obtained biochars were stored in airtight borosilicate glass vials (70 mL) and used for subsequent characterization and adsorption studies.

3.3.2   Characterization of the Biochar

The porosity and specific surface of AFB were analyzed *via* nitrogen adsorption/desorption isotherm at 77 K (the biochar sample was degassed before measurement *via* helium for 3 h at 553 K) through the BET methodology using a micrometer (TriStar II 3020 V1.03, USA). Scanning electron microscopy was utilized to survey the visual characteristics of the AFB surface (SEM, EVO 18 research SEM, Germany). The KBr pellet method was adopted to recognize the functionalities existing on the AFB samples through Fourier transform infrared (FTIR) spectroscopy (Thermo-Fisher FTIR analyzer Nicolet 5700, Japan) in the 400–4000 cm^{-1} range. The method of solid addition method was adopted to ascertain the point of zero charge (pH$_{ZPC}$) of the biochar sample (Cheng et al. 2015). Essentially, a series of solutions (0.1 g AFB dissolved in 100 mL 0.01 M NaCl solution) were prepared in 150-mL Erlenmeyer flasks. The initial pH (pH$_i$) of the solutions were regulated in the range of 2–12 by the addition of suitable amounts of 0.1 M NaOH and 0.1 M HCl. The solution pH was measured *via* a digital pH meter (Ion/pH meter metrohm model-691, USA) in two replicates. A rotary shaker was used to agitate the prepared solutions at 200 rpm and 298 K for 24 h. The resulting suspensions were subse-

quently filtered, and the final solution pH (pH_f) of the filtrates was determined upon the attainment of equilibrium. A plot between pH_f and pH_i was drawn to measure the pH_{ZPC} of AFB.

3.3.3   Dye Solution

CR (analytical grade, 99% pure) was procured from Sigma-Aldrich, India. The stock solution of CR (1000 mg/L) ($C_{32}H_{22}N_6Na_2O_6S_2$, MW: 696.66 g/mol) was made with Milli-Q water, whereas the desired concentrations for batch adsorption experiments were prepared as per requirement *via* successive dilutions. The concentration of dye was determined *via* a spectrophotometer (UV-Vis, HACH DR5000, Canada) at the maximum wavelength (λ_{max}) of 497 nm for the adsorption studies. The detection limit for CR dye was determined to be 0.049 ppm with a relative standard deviation (RSD) of 0.39% (or relative standard error of 0.22%).

3.3.4   Batch Adsorption Experiments

The sorption behavior of CR on AFB was investigated using batch mode experiments to study the effects of operating conditions (e.g., solution pH, biochar dosage, initial CR concentration, temperature, and contact time), implementing a single condition at a particular time. The values of these operating conditions were as follows: pH, 2–1; AFB dosage, 4–14 g/L; initial CR concentration, 20–100 mg/L; contact time, 30–480 min; and temperature, 30–60 °C. CR solutions (100 mL) with a predetermined quantity of AFB were added to Erlenmeyer flasks (125 mL). Standard experimental conditions of AFB dosage (w = 12 g/L), CR concentration (C_o = 50 mg/L), shaking speed (100 rpm), contact time (t = 3 h), temperature (30 ± 2 °C), and pH (7.0 ± 0.1) were utilized in all the batch experiments unless mentioned otherwise.

   A constant temperature shaking system was used to equilibrate the AFB and CR suspensions. After the experiment was completed, the resultant solution samples were decanted and centrifuged for 30 min at 1832 × *g*. The supernatant collected from centrifuged samples were used to analyze the concentration of residual CR *via* a UV-Vis spectrophotometer (HACH DR5000, Canada) at the maximum wavelength (λ_{max}) of 497 nm. The efficiency of removal (R %) and sorption capacity (q) were determined accordingly:

$$R(\%) = \frac{(C_o - C_e) \, x \, 100}{C_o} \tag{3.1}$$

$$q = \frac{(C_o - C_e) x V}{m} \tag{3.2}$$

where C_o (mg/L) is the initial concentration of CR, C_e (mg/L) is the equilibrium concentration of CR, V (L) is solution volume, and m (g) is the biochar dosage.

3.4 Experimental Case Study – Results and Discussion

3.4.1 Biochar Characterization and Dye Interaction

In Fig. 3.1a and b, the surface morphology of AFB was examined before and after adsorption, respectively using SEM micrograph images. Figure 3.1a shows that the surface morphology of the fresh AFB was relatively porous and irregular with a massive surface area for a surface interaction with CR. The SEM micrograph image of dye-loaded AFB shown in Fig. 3.1b confirmed that the surface became saturated with the dye (i.e., most pores covered with CR molecules) after adsorption. According to the characterization results of the biochar, the BET specific surface, average pore width, and net pore volume of Arjun fruit were 770.68 m^2/g, 2.89 nm, and 0.4 cm^3/g, respectively.

The FTIR spectra of AFB in Fig. 3.2a and b show various characteristic peaks. These peaks represent different functionalities present on the AFB surface. The wide band at 3387 cm^{-1} resembled the hydrogen bonded OH groups of alcohol and H-bonded N-H group (Amir et al. 2010). However, the band underwent a shift to 3385 cm^{-1} after adsorption of CR onto the AFB surface owing to the interaction of the O-H bond of AFB with the $-N^-$ bond of CR. The band perceived at 2337 cm^{-1} belonged to the stretching vibrations of C=O bond of the CO_2 molecule, which was shifted to 2348 cm^{-1} with a simultaneous increase in the intensity of the peak, indi-
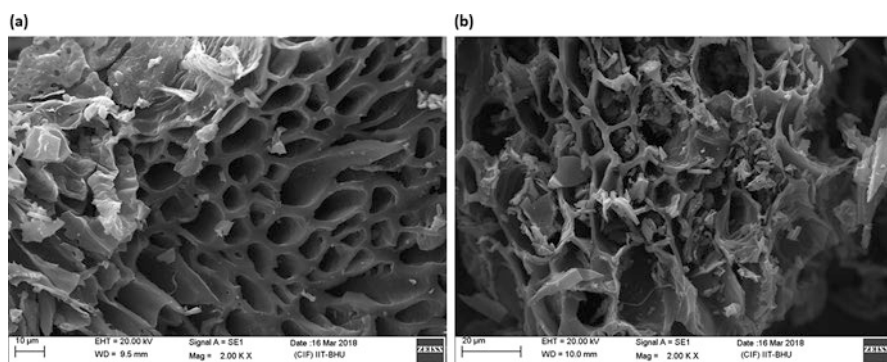

Fig. 3.1 Scanning electron microscopy images of Arjun fruit biochar. (**a**) Before and (**b**) after adsorption of Congo red
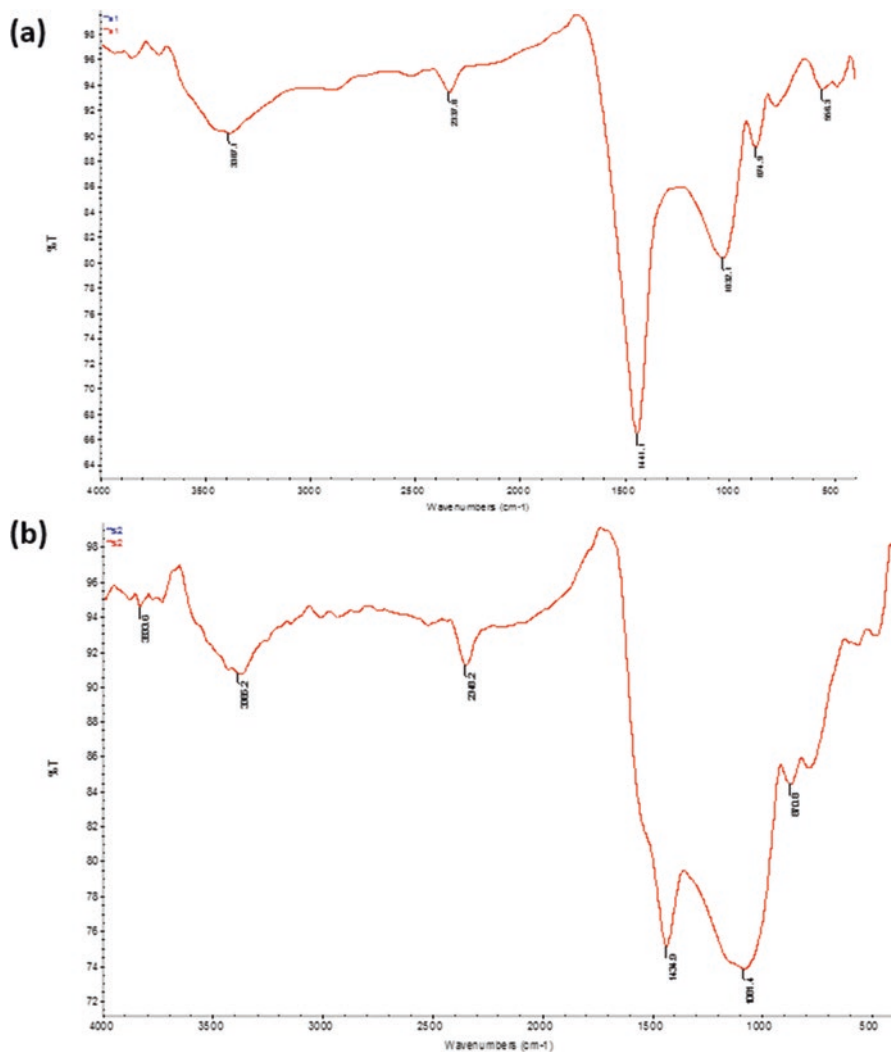
Fig. 3.2 Fourier-transform infrared spectroscopy spectra of Arjun fruit biochar before and after dye adsorption. (**a**) Before adsorption. (**b**) After adsorption

cating a rise in the CO_2 concentration after the sorption process (Pachecka et al. 2017). Another prominent band was perceived at 1441 cm^{-1} and belonged to the O-H of phenol, COO^- (Amir et al. 2010). This band also resulted in a shift to 1439 cm^{-1} because of the adsorption of the CR dye. The shift indicates the participation of the COO^- of AFB in the adsorption mechanism. Furthermore, the stretching band at 1332 cm^{-1} corresponded to the vibrations of the CO bond, which surprisingly shifted to 1081 cm^{-1} with a wider peak. This was due to an increase in the concentration of CO bond vibrations after the adsorption of CR. The absorption

peaks at 874 cm^{-1} showcased the existence of a [CO$_3$] functionality in the AFB, which decreased in concentration after adsorption as the peak reduced to 870 cm^{-1} (Fleet and Liu 2007). These interactions amongst the functionalities present in AFB and CR dye molecule could form weak van der Waals bonds or hydrogen bonds to improve the adsorption capacity and performance of AFB.

3.4.2   Batch Adsorption Experiments

3.4.2.1   Effects of Solution pH

The solution pH boosts the sorption of dye molecules on the biochar in multiple ways such as fluctuation in the biochar surface charge and dye molecule ionization. These two phenomena govern the mass transfer between the biochar surface and dye molecules. As a result, information on the optimum pH is imperative in precisely describing the adsorption process (Yu et al. 2018; Zazycki et al. 2018). The solution pH was regulated in the range of 2–12 through the addition of 0.1 M NaOH and 0.1 M HCl. The maximal efficiency of dye removal (96.3%) and sorption capacity of the sorbent (4.81 mg/g) were obtained at the solution pH of 2 ± 0.1 (Fig. 3.3).

The variation in the pH of aqueous solution was also observed after the sorption of CR on AFB (Fig. 3.4). As the initial CR solution pH (pH$_i$) fluctuated from 2 to 8, the final pH of CR solution at equilibrium (pH$_f$) was larger than the corresponding pH$_i$ values. The point of zero charge (pH$_{ZPC}$) of AFB can be utilized to evaluate the impact of solution pH on CR sorption. As shown in Fig. 3.4, the pH$_{ZPC}$ of AFB was 8.1. The surface of AFB is positively charged at pH values lower than pH$_{ZPC}$. The findings of high efficiency of dye removal and biochar sorption capacity may be ascribed to the prospective electrostatic attraction amongst CR anions and the posi-
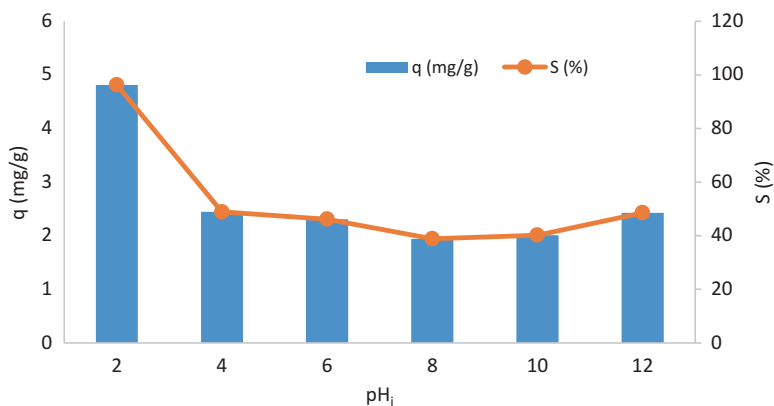

Fig. 3.3 Effect of solution pH on the adsorption of Congo red on Arjun fruit biochar (T = 30 ± 2 °C, C$_o$ = 50 mg/L, w = 10 g/L, t = 3 h, and agitation speed = 100 rpm)
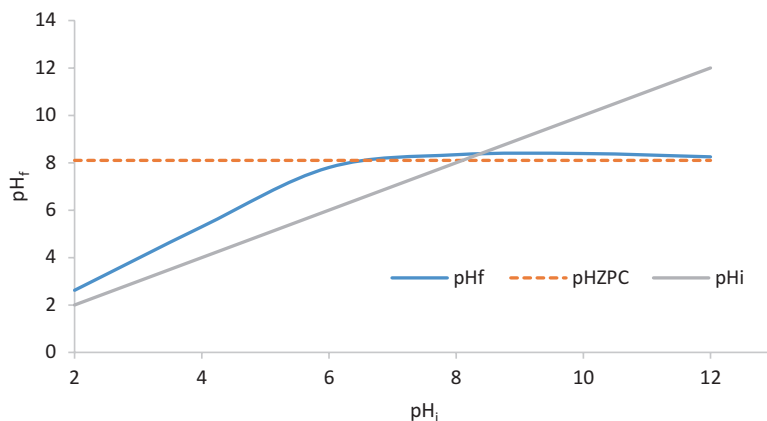
Fig. 3.4 Point of zero charge of Arjun fruit biochar (T = 30 ± 2 °C, C_o = 50 mg/L, w = 10 g/L, t = 3 h, and agitation speed = 100 rpm)

tively charged AFB surface. The adsorption of CR by orange peel powder was observed to be maximum at a pH of 3 (Munagapati and Kim 2016). The adsorbent surface acquired a positive charge at the low pH where the elevated adsorption of CR anions takes place. The pH of industrial effluents rich in CR is generally reported in the range from 7 to 11 (Gharbani et al. 2008). Moreover, as pH adjustments require a significant amount of chemicals, it may render the treatment process highly uneconomical (Jiang et al. 2018; Molinos-Senante and Guzmán 2018). Considering all the above-mentioned factors, the subsequent experiments were operated at a pH of 7 ± 0.1. As this pH value is lower than pH_{ZPC}, a positively charged biochar surface is made to provide a practical and economical solution for the abatement of dyes from water/wastewater.

3.4.2.2 Effects of Contact Time and Initial Dye Concentration

The initial concentration of a dye solution and contact time are key parameters for designing adsorption-based wastewater treatment systems (Oladoja et al. 2017). The effects of initial dye concentration (20–100 mg/L) and contact time (30–480 min) on the sorption behavior and sorbent capacity are shown in Fig. 3.5.

The sorption capacity increased from 0.8 to 1.72 mg/g when the primary CR concentration changed from 20 to 100 mg/L. Two stages of the adsorption were observed when CR was uptaken by the AFB. The adsorption capacity of AFB elevated rapidly in the initial 30 min with a subsequent slow sorption period, throughout which the AFB sorption capacity slowly rises from 30 min to 120 min. No substantial enhancement was observed after the increase. This two-stage adsorption (rapid adsorption followed by slow adsorption) was also observed for the adsorption of brilliant green dye on biochar produced from hydrolyzed rice straw (Saif Ur
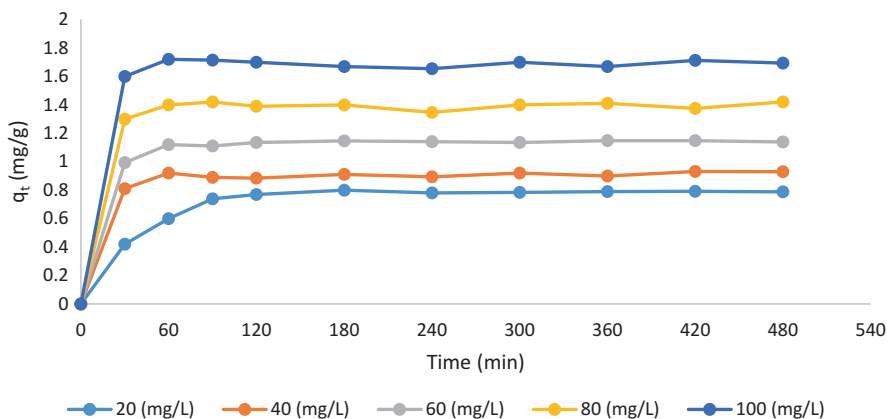
Fig. 3.5 Effect of contact time on the adsorption of Congo red on Arjun fruit biochar (T = 30 ± 2 °C, pH 7.0 ± 0.1, w = 12 g/L, agitation speed = 100 rpm)

Rehman et al. 2016). At low initial concentrations, few CR molecules cover the external active sites of the AFB surface through boundary layer adsorption. However, most external active sites remain uncovered owing to the low availability of CR molecules in the solution. Conversely, at high initial concentrations, a significant amount of available external active sites decreased with time, and the CR molecules reached the internal sites of the AFB through diffusion. Therefore, a slow adsorption process was seen in the second stage until equilibrium was achieved (Oladipo and Ifebajo 2018; Yu et al. 2018).

3.4.2.3 Effects of Biochar Dosage

The effects of the AFB dosage on the adsorption performance are shown in Fig. 3.6. The AFB dosage varied from 4 to 14 g/L. An opposite trend was observed for adsorption efficiency and capacity with an increase in the AFB dosage. The removal efficiency rose from 32.5% to 40%, while the sorption capacity was observed to decrease from 4.07 to 1.29 mg/g. The adsorption capacity of rice straw biochar for brilliant green reduced from 277 mg/g to 20 mg/g when the biochar dosage increased from 0.05 g/L to 1.25 g/L (Saif Ur Rehman et al. 2016). The removal efficiency of kenaf fiber biochar for methylene blue removal significantly increased from 48% to 76% when the biochar dosage was varied from 0.2 to 0.5 g/L (Mahmoud et al. 2012). Equations 3.1 and 3.2 can be used effectively to describe the observed opposite trends. The net amount of CR molecules was fixed (C_o = 50 mg/L) against an increasing AFB dosage (4–14 g/L). As a consequence, the number of CR molecules adsorbed per unit mass of AFB was reduced resulting in a low adsorption capacity; hence, a large number of active sites were left uncovered at high AFB dosage (Sadaf and Bhatti 2014). An elevation in the AFB dosage gradually increased the CR
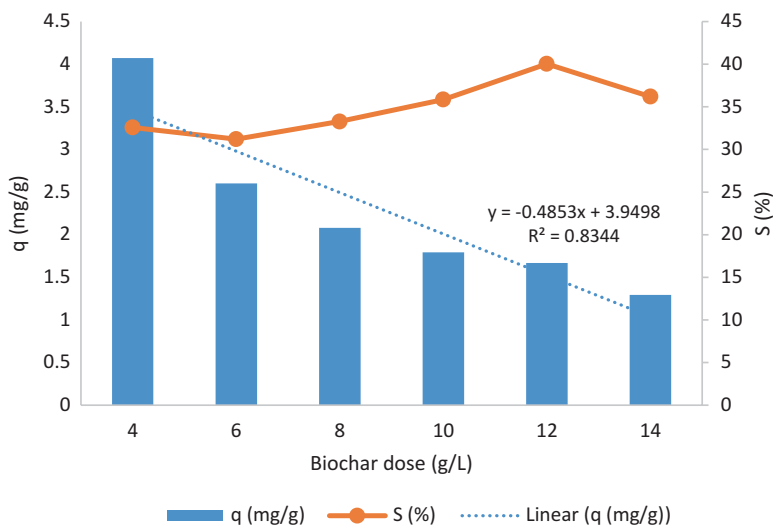
Fig. 3.6 Effect of biochar dosage on the adsorption of Congo red on Arjun fruit biochar ($T = 30 \pm 2$ °C, pH 7.0 ± 0.1, $C_o = 50$ mg/L, t = 3 h, agitation speed = 100 rpm)

uptake (C_o-C_e) and consequently elevated the removal efficiency (Eq. 3.1). However, q_e was lower than R (%) because the AFB dosage (w) was present in the denominator of Eq. 3.2, resulting in an inverse relation between q and w (Zazycki et al. 2018). Subsequent experiments were conducted using 12 g/L of AFB to achieve the highest CR removal.

3.4.2.4 Effects of Temperature

Temperature plays a detrimental role in adsorption because the adsorption capacity at equilibrium is highly dependent on temperature fluctuations (Vikrant et al. 2018). The AFB adsorption capacity increased from 1.66 mg/g to 2.16 mg/g when the temperature rose from 30 °C to 60 °C, suggesting the endothermic character of the sorption process (Fig. 3.7).

The elevated sorption capacity could be attributed to the temperature-mediated increase in the amount of active sites on the AFB surface (Santos et al. 2017). Also, this phenomenon could be attributed to the increased mobility of CR molecules coupled with their heightened affinity toward the binding sites that are available on the AFB surface (Zhang et al. 2017). A similar endothermic adsorption of CR on cationic modified orange peel powder was reported previously (Munagapati and Kim 2016); a relatable endothermic character was also perceived for the sorptive removal of methylene blue by acid treated kenaf fiber char (Mahmoud et al. 2012).
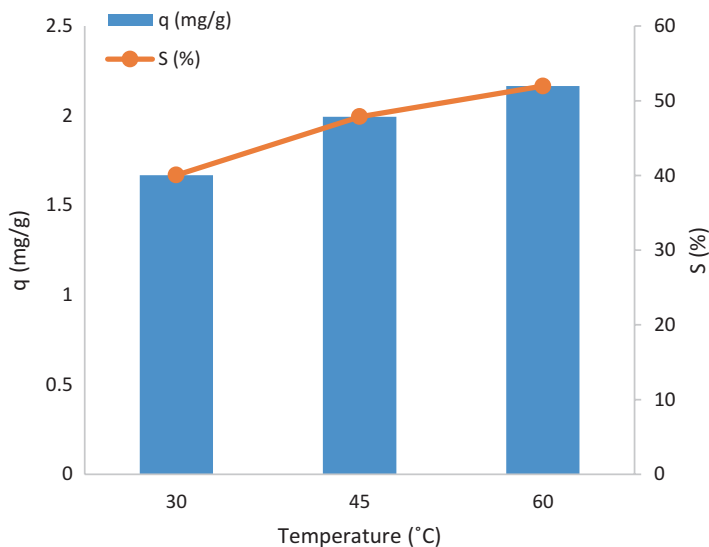
Fig. 3.7 Effect of temperature on the adsorption of Congo red on Arjun fruit biochar (pH 7.0 ± 0.1, C_o = 50 mg/L, t = 3 h, w = 12 g/L, agitation speed = 100 rpm)

3.4.3 Adsorption Kinetics

Adsorption kinetic investigations supplies into adsorption mechanisms. Commonly used models, namely Lagergren pseudo-first order (Eq. 3.3), pseudo-second order (Eq. 3.4), and intra-particle diffusion (Eq. 3.5) models, were used to analyze the prospective adsorption mechanisms (Vikrant et al. 2018).

$$\log\left(q_e - q_t\right) = \log q_e - \frac{k_1 t}{2.303} \tag{3.3}$$

$$\frac{t}{q_t} = \frac{1}{\left(k_2\right)\left(q_e\right)^2} + \frac{t}{q_e} \tag{3.4}$$

$$q_t = K_{pi} t^{\frac{1}{2}} + C_i \tag{3.5}$$

where q_t is the sorption capacity (mg/g) at any instant t, k_1 (min^{-1}) is the first order sorption rate constant, k_2 (g.(mg.min)$^{-1}$) is the second order sorption rate constant, h = $k_2 q_e^2$ depicts the initial sorption rate (mg.(g.min)$^{-1}$), C_i (mg/g) represents the thickness of boundary layer, and K_{pi} (mg.(g.min)$^{-1/2}$) denotes the intra-particle diffusion rate constant. Table 3.1A summarizes the kinetic parameters for CR adsorption on AFB. The pseudo-first order kinetics did not fit well for the obtained batch

Table 3.1 Adsorption parameters of Congo red dye on Arjun fruit biochar. (A) Kinetics, (B) isotherm, and (C) thermodynamics

[A] Kinetics

Order	Dye Conc. (mg/L)	q_{exp} (mg/g)	Pseudo-first order parameter				Pseudo-second order parameter			Intra-particle diffusion parameter			
			k_1 (h^{-1})	q_{cal} (mg/g)	R^2	q_{DEV} (mg/g)	k_2 (g/mgh)	q_{cal} (mg/g)	R^2	q_{DEV} (mg/g)	K_{pi}	C_i	R^2
1	20	0.77	0.00852	0.2652	0.8045	0.5048	0.1041	0.8146	0.9977	0.0446	0.0301	0.2743	0.6841
2	40	0.884	0.00806	0.1418	0.5668	0.7422	0.2912	0.9289	0.9994	0.0449	0.0274	0.465	0.4697
3	60	1.135	0.00783	0.0833	0.3449	1.0517	0.4567	1.1487	0.9999	0.0137	0.0344	0.5782	0.4731
4	80	1.39	0.00898	0.2113	0.5154	1.1787	0.527	1.4029	0.9993	0.0129	0.0399	0.7479	0.4209
5	100	1.698	0.00484	0.1211	0.2443	1.5769	0.7115	1.6955	0.9997	0.0025	0.0475	0.9197	0.4068

[B] Isotherm

Order	Langmuir				Freundlich		
	R^2	q_m (mg/g)	K_a (L/mg)	R_L	R^2	K_f (mg/g)	n
1	0.998	2.534	0.411	0.023–0.108	0.257	16.683	0.413

[C] Thermodynamics

Order	Temperature (°C)	$-\Delta G$ (kJ Mol^{-1})	ΔH (kJ Mol^{-1})	ΔS (kJ Mol^{-1})
1	30	3.161	5.886	0.009
2	45	2.951		
3	60	2.893		

Fig. 3.8 Pseudo-second order kinetic model of Congo red on Arjun fruit biochar (T = 30 ± 2 °C, pH 7.0 ± 0.1, C_o = 20–100 mg/L, t = 3 h, w = 12 g/L, agitation speed = 100 rpm)

adsorption data because the R^2 values ranged between 0.2443 and 0.8045 along with a large absolute deviation of the experimental adsorption capacity (q_{DEV}) (0.5048–1.5769 mg/g), whereas the pseudo-second order kinetics fits the adsorption data exceptionally well ($R^2 > 0.9977$) (Fig. 3.8). The q_{DEV} values were obtained by using Eq. 3.6.

$$q_{DEV} = \left| q_{e,\exp} - q_{e,cal} \right| \qquad (3.6)$$

Where $q_{e,\exp}$ represents the experimental sorption capacity (mg/g) and $q_{e,cal}$ denotes the calculated sorption capacity (mg/g). High correlation coefficients (R^2) indicate that the pseudo-second order model shows a better fit than other models to explain the sorption of CR on AFB. Along similar lines, the pseudo-second order model fitted the sorption of CR onto cationic modified orange peel powder (Munagapati and Kim 2016), ZnO-modified SiO_2 nanospheres (Zhang et al. 2018), and chestnut husk-like $NiCo_2O_4$ hollow microspheres (Chen et al. 2018) with high accuracy.

For a better understanding of sorption kinetics, the intra-particle diffusion model was also fitted to the kinetics data (Table 3.1A). The R^2 values for the intra-particle diffusion kinetic model were in the range of 0.4068–0.6841, indicating its non-applicability. The C_i values (0.2743–0.9197) indicate the contribution of pore diffusion to a limited extent toward adsorption of CR on AFB. However, these values may not be the only rate-determining stage involved in the sorption activity (e.g., rapid film adsorption may also be involved) (Mane et al. 2007; Mane and Babu

2011). Similar observations were also reported for the abatement of brilliant green dye by hydrolyzed rice straw (Saif Ur Rehman et al. 2016).

3.4.4 Adsorption Isotherms

Investigations on sorption equilibrium are necessary to learn how to optimize and scale up adsorption-based wastewater treatment systems (Molinos-Senante and Guzmán 2018). Langmuir (Eq. 3.7) and Freundlich (see supplementary information and Table 3.1B) isotherm models were utilized to analyze the data obtained from batch experiments.

$$\frac{C_e}{q_e} = \frac{C_e}{q_m} + \frac{1}{K_a q_m}$$

(3.7)

Where q_m represents the maximum monolayer sorption capacity and K_a is the Langmuir sorption equilibrium constant (L/mg).

Figure 3.9 and Table 3.1(B) show the Langmuir isotherm profile and associated parameters, respectively. The very high R^2 value (0.9985) indicates that Langmuir model should be more fitting than various other models to analyze the sorption of CR at equilibrium condition. A separation factor (R_L) value in the range of 0 to 1 also indicates the feasibility of adsorption of CR onto AFB (Eq. 3.8) (Saif Ur Rehman et al. 2016).
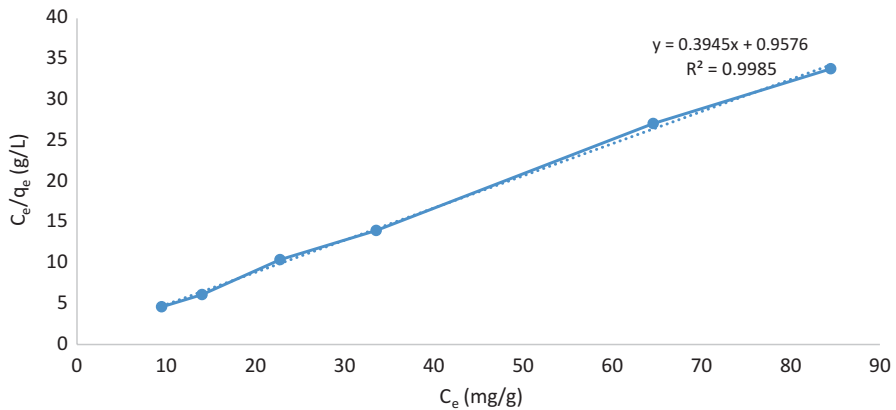
$$R_L = \frac{1}{\left(1 + K_a C_o\right)}$$

(3.8)

Fig. 3.9 Langmuir isotherm model fitted to the data of Congo red adsorption on Arjun fruit bio-char (T = 30 ± 2 °C, pH 7.0 ± 0.1, C_o = 20–100 mg/L, t = 3 h, w = 12 g/L, agitation speed = 100 rpm)

Table 3.2 Comparison between different biomass-based adsorbents for the removal of Congo red dye

Order	Adsorbent	Max. Adsorption efficiency (%)	Max. Adsorption capacity (mg/g)	pH	References
1	Jute stick powder	–	35.7	7	Panda et al. (2009)
2	Sugarcane bagasse	89.9	38.2	5	Zhang et al. (2011)
3	Rubber seeds	98.4	9.82	6	Zulfikar et al. (2015)
4	Modified orange peel powder	–	163	3	Munagapati and Kim (2016)
5	Arjun fruit biochar	96.25	4.81	2	This study

The calculated R_L values were observed to be in the range of 0.023–0.108 for all tested concentrations, thus confirming that CR could be successfully removed by adsorption on AFB. The Langmuir isotherm was also a good fit for CR adsorption onto cationic modified orange peel powder (Munagapati and Kim 2016) and chestnut husk-like $NiCo_2O_4$ hollow microspheres (Chen et al. 2018). These findings suggest that a monolayer adsorption was prevalent. The formation of a monolayer can be attested by calculating the coverage factor (θ), which is given by Eq. 3.9.

$$\theta = \frac{\left[q_m N \sigma 10^{-20} \right]}{S_{BET}} \tag{3.9}$$

The value of θ varies between 0 (no coverage) to 1 (full coverage). The θ value was 0.68, which confirms the formation of a monolayer. The partial coverage of the AFB surface occurred because CR is a large sized molecule, which can obstruct its movement onto the micropores (Al-Degs et al. 2008). A comparison between the performance of processes from different studies on the adsorptive removal of CR is summarized in Table 3.2.

3.5   Adsorption Thermodynamics

The following equations were utilized to analyze the thermodynamics of CR sorption onto AFB (Munagapati and Kim 2016):

$$\Delta G = -RTlnK \tag{3.10}$$

$$lnK = \frac{\Delta S}{R} - \frac{\Delta H}{RT} \tag{3.11}$$

where R is the ideal gas constant (8.314 J mol^{-1} K^{-1}), T (K) is the absolute temperature, $K = q_e/C_e$, ΔG is the Gibbs free energy, ΔS is the entropy change, and ΔH is the enthalpy change. The values of ΔS and ΔH were calculated from the intercept

and slope of lnK vs. 1/T (Saif Ur Rehman et al. 2016). ΔG values were calculated using Eq. 3.10. The feasibility and spontaneity of CR adsorption on AFB were affirmed by the negative values of ΔG at all tested temperatures (30–60 °C) (Table 3.1C) (Mane et al. 2007). The ΔG value continuously decreased for a rise in the solution temperature, thereby indicating the endothermic tendency of the sorption process as elucidated in Sect. 3.4.2.4. The values of ΔG were observed to be in the −20–0 kJ mol⁻¹ range, suggesting that CR sorption on AFB is a physically driven process (Zhang et al. 2018).

The positive value of ΔH (i.e., +5.886 kJ mol⁻¹) confirms the endothermic character of the adsorption process. ΔH values can be used to understand the physical adsorption of analytes on adsorbents such as 5 kJ mol⁻¹ (hydrophobic bonding), 4–10 kJ mol⁻¹ (van der Waals forces), 2–40 kJ mol⁻¹ (hydrogen bonding), 2–29 kJ mol⁻¹ (dipole bonding), and 40 kJ mol⁻¹ (coordination exchange) (Saif Ur Rehman et al. 2016). Based on this classification, the ΔH value of CR adsorption on AFB affirms its physical nature and suggests there is a complex combination of van der Waals, hydrophobic, dipole, and hydrogen bonding forces. The positive ΔS value (+0.009 kJ mol⁻¹) indicates that a temperature increase should have promoted CR adsorption by dislocating the water molecules present on the biochar surface (Auta and Hameed 2012). The adsorption of CR on cationic modified orange peel powder was also spontaneous and endothermic (Munagapati and Kim 2016). However, the thermodynamic analysis of CR adsorption onto ball-milled sugarcane bagasse implies that the process is spontaneous and exothermic (Zhang et al. 2011). Interestingly, the sorption of CR onto rubber seeds was observed to be endothermic and non-spontaneous (Zulfikar et al. 2015). It can be perceived that the sorption thermodynamic results are indispensable toward the detailed understanding of sorption behavior as well as investigating the spontaneity of the process.

3.5.1   Desorption and Regeneration Experiments

Desorption studies showcase the regenerative ability of adsorbents and the potential of recovering dye molecules. The selection of proper eluents is important for a successful desorption operation. The choice of eluents is typically based upon the type of adsorption mechanism and the nature of the adsorbent. For the desorption experiment, various eluents were prepared such as 0.1 M NaOH, 0.1 M CH₃COOH, deionized water, and 0.1 M HCl. Figure 3.10a presents the results of desorption investigations. The superior eluent, when compared to three other eluents, was noted to be 0.1 M NaOH, which displayed a CR recovery of 86%.

The regeneration of biochar is favorable from a financial perspective and for the recovery of dye molecules. Based on the results of Fig. 3.10a, 0.1 M NaOH was utilized as the eluent for regeneration cycle experiments (Fig. 3.10b). A progressive reduction in CR sorption capacity was observed for AFB with a rise in the number of regeneration cycles. After the subsequent five cycles, the CR desorption capacity of AFB decreased from 86% to 79%. The decrease in the sorption capacity was
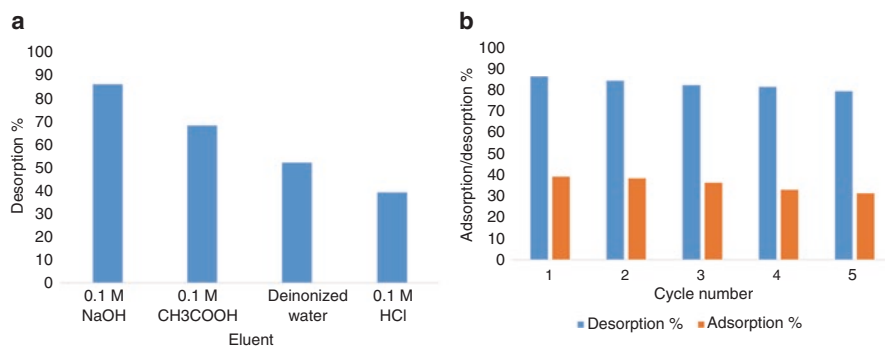
Fig. 3.10 Desorption studies of Congo red. (**a**) Desorption; (**b**) Number of adsorption-desorption cycles

found to be less than 10% which might be a consequence of biochar loss during the regeneration process. As a result, AFB can be used for at least five cycles of CR adsorption effectively.

3.6   Adsorption Mechanisms

The adsorption of CR onto the surface of AFB can be mainly explained by three forces, namely electrostatic, Van der Waals, and hydrogen bonding. Observed two probable mechanisms for adsorption of CR onto coir pith carbon, including (1) electrostatic adsorption owing to the interactions amongst the positive charge bearing protonated functionalities of carbon and the negatively charged deprotonated acidic dye, and (2) the physical adsorption or chemical reaction amongst the adsorbate and adsorbent. Analogous adsorption processes might also occur during the adsorption of CR onto AFB.

Figure 3.11 shows the adsorption mechanism of CR onto AFB in solutions of different pH (acidic, neutral, and alkaline). In the solution with a pH below pH_{ZPC}, the surface of the AFB was positively charged. This highly favors the electrostatic interactions amongst the AFB surface (bearing positive charge) and the anionic CR molecules with SO_3^- as a functional group. The FTIR analysis of the AFB discloses the presence of acidic functionalities (e.g., hydroxyls and carboxyls), which should primarily furnish the electrostatic interactions amongst the SO_3^- group of CR and the functional groups of AFB at acidic conditions. When the solution pH changed from acidic to alkaline, the number of positively charged sites of AFB decreased. The shift in solution pH resulted in an increase of negatively charged surface sites. This phenomenon resulted in the repulsion of the AFB surface and anionic dye. However, Fig. 3.3 shows outstanding removal efficiency and maximum adsorption capacity at a high pH. Hence, the adsorption can be physically controlled when the solution is alkaline. This physisorption process was also supported by the ΔG val-
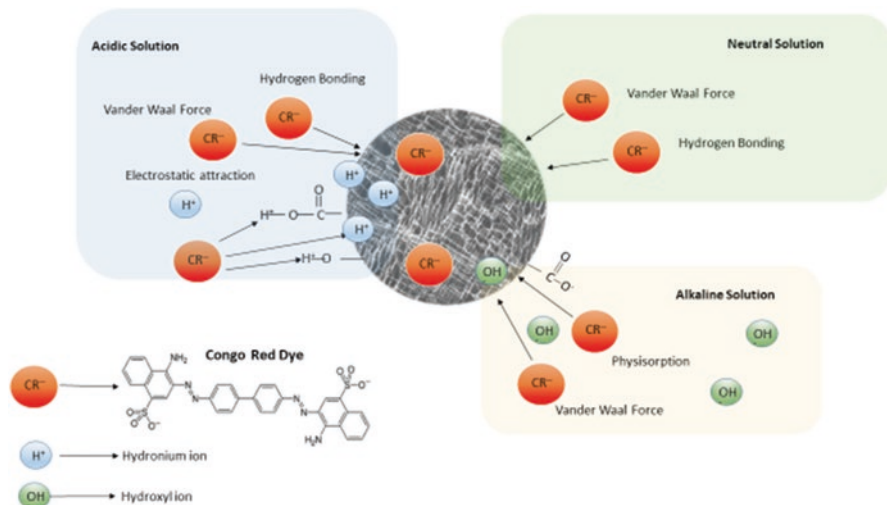
Fig. 3.11 Proposed adsorption mechanism for Congo red dye on the Arjun fruit biochar surface at different pH conditions

ues obtained in Sect. 3.6. The FTIR data also demonstrate a change in the band from 3387 cm^{-1} to 3385 cm^{-1} after the sorption of CR onto AFB due to the interaction of the O-H bond of AFB with the –N$^-$ bond of CR. Another band at 1441 cm^{-1} underwent a shift to 1439 cm^{-1}, showing the participation of the COO$^-$ group of AFB. The drastic change in the peak from 1032 cm^{-1} to 1081 cm^{-1} clearly explains the adsorption of CR onto the AFB surface. The shift in the peaks of FTIR data is likely to reflect the formation of new bonds for weak van der Waals forces and hydrogen bonding between the functional groups of the AFB and CR dye molecule. Also, the transfer of the CR molecules from the bulk of aqueous solution to the AFB surface might contain these four steps: (1) transport of CR molecule from the bulk aqueous solution to the AFB surface, (2) transfer of CR molecules to the AFB surface through diffusion across the boundary layer, (3) adsorption at the surface sites of the sorbent, and (4) intra-particular diffusion through the surface of the sorbent (Sen et al. 2011).

3.7 Conclusions

Till date, varied physicochemical treatment options have been designed for the removal of dyes. However, the performance of these conventional systems is limited due to high cost, large energy and chemical requirements, generation of sludge and toxic byproducts. This chapter acknowledges adsorption as an apt option for the removal of dyes, due to their advantageous properties such as environmental benignity, economical operation, easy and safe operation, and no sludge generation. The experimental case study showcased the applicability of a biochar derived from the

fruit of *T. arjuna* as an efficacious sorbent for the abatement dyes from water/wastewater. The maximum removal efficiency and adsorption capacity of CR by AFB were 96.25% and 4.81 mg/g, respectively. The kinetic, equilibrium, and thermodynamic analyses of the adsorption process revealed that CR sorption on AFB is a spontaneous and feasible method that is physical in nature. The reusability of biochar was reliable with minimal loss of adsorption capacity when tested over five regeneration cycles. The experimental observations of the present investigation showcased that the fruit of *T. arjuna*, which remains largely unused by the pharmaceutical industry, can be used in treatment facilities for the efficient removal of pigments and dyes from water/wastewater. Such innovative usage of indigenously produced waste biomass holds a great potential for sustainable waste management as well as a cost-effective pollution control process.

References

Abu Talha M, Goswami M, Giri BS, Sharma A, Rai BN, Singh RS (2018) Bioremediation of Congo red dye in immobilized batch and continuous packed bed bioreactor by Brevibacillus parabrevis using coconut shell bio-char. Bioresour Technol 252:37–43

Al-Degs YS, El-Barghouthi MI, El-Sheikh AH, Walker GM (2008) Effect of solution pH, ionic strength, and temperature on adsorption behavior of reactive dyes on activated carbon. Dyes Pigments 77:16–23

Amalraj A, Gopi S (2017) Medicinal properties of Terminalia arjuna (Roxb.) Wight & Arn.: a review. J Tradit Complement Med 7:65–78

Amir S, Jouraiphy A, Meddich A, El Gharous M, Winterton P, Hafidi M (2010) Structural study of humic acids during composting of activated sludge-green waste: elemental analysis, FTIR and 13C NMR. J Hazard Mater 177:524–529

Auta M, Hameed BH (2012) Modified mesoporous clay adsorbent for adsorption isotherm and kinetics of methylene blue. Chem Eng J 198-199:219–227

Bangash Fazlullah K, Manaf A (2013) Dyes removal from aqueous solution using wood activated charcoal of Bombax Cieba tree. J Chin Chem Soc 52:489–494

Bello OS, Ahmad MA (2012) Coconut (Cocos nucifera) Shell based activated carbon for the removal of malachite green dye from aqueous solutions. Separation Sci Technol 47:903–912

Brüschweiler BJ, Merlot C (2017) Azo dyes in clothing textiles can be cleaved into a series of mutagenic aromatic amines which are not regulated yet. Regul Toxicol Pharmacol 88:214–226

Chen H, Zheng Y, Cheng B, Yu J, Jiang C (2018) Chestnut husk-like nickel cobaltite hollow microspheres for the adsorption of Congo red. J Alloys Comp 735:1041–1051

Cheng Z, Zhang L, Guo X, Jiang X, Li T (2015) Adsorption behavior of direct red 80 and congo red onto activated carbon/surfactant: process optimization, kinetics and equilibrium. Spectrochim Acta A Mol Biomol Spectrosc 137:1126–1143

Chung KT (2016) Azo dyes and human health: a review. J Environ Sci Health C Environ Carcinog Ecotoxicol Rev 34:233–261

D'Inverno G, Carosi L, Romano G, Guerrini A (2018) Water pollution in wastewater treatment plants: an efficiency analysis with undesirable output. Eur J Oper Res 269:24–34

Doulati Ardejani F, Badii K, Limaee NY, Shafaei SZ, Mirhabibi AR (2008) Adsorption of Direct Red 80 dye from aqueous solution onto almond shells: effect of pH, initial concentration and shell type. J Hazard Mater 151:730–737

Dwivedi S, Chopra D (2014) Revisiting Terminalia arjuna – An Ancient Cardiovascular Drug. J Tradit Complment Med 4:224–231

El-Sonbati AZ, El-Deen IM, El-Bindary MA (2016) Adsorption of hazardous Azorhodanine dye from an aqueous solution using Rice Straw Fly Ash. J Dispers Sci Technol 37:715–722

Fleet ME, Liu X (2007) Coupled substitution of type A and B carbonate in sodium-bearing apatite. Biomaterials 28:916–926

Gharbani P, Tabatabaii SM, Mehrizad A (2008) Removal of Congo red from textile wastewater by ozonation. Int J Environ Sci Technol 5:495–500

Jayapal M, Jagadeesan H, Shanmugam M, Danisha JP, Murugesan S (2018) Sequential anaerobic-aerobic treatment using plant microbe integrated system for degradation of azo dyes and their aromatic amines by-products. J Hazard Mater 354:231–243

Jiang Y, Dinar A, Hellegers P (2018) Economics of social trade-off: balancing wastewater treatment cost and ecosystem damage. J Environ Manag 211:42–52

Kumar A, Singh JS (2017) Cyanoremediation: a green-clean tool for decontamination of synthetic pesticides from agro-and aquatic ecosystems. In: Singh JS, Seneviratne G (eds) Agro-environmental sustainability: Vol (2) managing environmental pollution. Springer, Cham, pp 59–83

Kumar A, Kaushal S, Saraf S, Singh JS (2017) Cyanobacterial biotechnology: an opportunity for sustainable industrial production. Clim Change Environ Sustain 5(1):97–110

Kumar A, Kaushal S, Saraf S, Singh JS (2018) Microbial bio-fuels: a solution to carbon emissions and energy crisis. Front Biosci (Landmark) 23:1789–1802

Leo L, Loong C, Ho XL, Raman MFB, Suan MYT, Loke WM (2018) Occurrence of azo food dyes and their effects on cellular inflammatory responses. Nutrition 46:36–40

Mahmoud DK, Salleh MAM, Karim WAWA, Idris A, Abidin ZZ (2012) Batch adsorption of basic dye using acid treated kenaf fibre char: equilibrium, kinetic and thermodynamic studies. Chem Eng J 181-182:449–457

Mane VS, Babu PVV (2011) Studies on the adsorption of Brilliant Green dye from aqueous solution onto low-cost NaOH treated saw dust. Desalination 273:321–329

Mane VS, Mall ID, Srivastava VC (2007) Use of bagasse fly ash as an adsorbent for the removal of brilliant green dye from aqueous solution. Dyes Pigments 73:269–278

Meerbergen K, Willems KA, Dewil R, Van Impe J, Appels L, Lievens B (2018) Isolation and screening of bacterial isolates from wastewater treatment plants to decolorize azo dyes. J Biosci Bioeng 125:448–456

Mekonnen Mesfin M, Hoekstra Arjen Y (2017) Global anthropogenic phosphorus loads to freshwater and associated Grey water footprints and water pollution levels: a high-resolution global study. Water Resour Res 54:345–358

Mella B, Barcellos BSC, da Silva Costa DE, Gutterres M (2018) Treatment of leather dyeing wastewater with associated process of coagulation-flocculation/adsorption/ozonation. Ozone Sci Eng 40:133–140

Molinos-Senante M, Guzmán C (2018) Benchmarking energy efficiency in drinking water treatment plants: quantification of potential savings. J Clean Prod 176:417–425

Munagapati VS, Kim D-S (2016) Adsorption of anionic azo dye Congo Red from aqueous solution by cationic modified Orange Peel powder. J Mol Liquids 220:540–548

Nidheesh PV, Zhou M, Oturan MA (2018) An overview on the removal of synthetic dyes from water by electrochemical advanced oxidation processes. Chemosphere 197:210–227

Oladipo AA, Ifebajo AO (2018) Highly efficient magnetic chicken bone biochar for removal of tetracycline and fluorescent dye from wastewater: two-stage adsorber analysis. J Environ Manag 209:9–16

Oladoja NA, Unuabonah EI, Amuda OS, Kolawole OM (2017) Operational principles and material requirements for coagulation/flocculation and adsorption-based water treatment operations. In: Oladoja NA, Unuabonah EI, Amuda OS, Kolawole OM (eds) Polysaccharides as a green and sustainable resources for water and wastewater treatment. Springer, Cham, pp 1–11

Pachecka M, Sturm JM, Lee CJ, Bijkerk F (2017) Adsorption and dissociation of CO2 on Ru(0001). J Phys ChemC 121:6729–6735

Panda GC, Das SK, Guha AK (2009) Jute stick powder as a potential biomass for the removal of congo red and rhodamine B from their aqueous solution. J Hazard Mater 164:374–379

Peydayesh M, Mohammadi T, Bakhtiari O (2018) Effective treatment of dye wastewater via positively charged TETA-MWCNT/PES hybrid nanofiltration membranes. Sep Purif Technol 194:488–502

Pham TD, Do TT, Ha VL, Doan THY, Nguyen TAH, Mai TD, Kobayashi M, Adachi Y (2017) Adsorptive removal of ammonium ion from aqueous solution using surfactant-modified alumina. Environ Chem 14:327–337

Pham T, Bui T, Nguyen V, Bui T, Tran T, Phan Q, Pham T, Hoang T (2018) Adsorption of polyelectrolyte onto Nanosilica Synthesized from Rice husk: characteristics, mechanisms, and application for antibiotic removal. Polymers 10:220

Sadaf S, Bhatti HN (2014) Batch and fixed bed column studies for the removal of Indosol Yellow BG dye by peanut husk. J Taiwan Inst Chem Eng 45:541–553

Saif Ur Rehman M, Kim I, Rashid N, Adeel Umer M, Sajid M, Han J-I (2016) Adsorption of brilliant green dye on biochar prepared from Lignocellulosic bioethanol plant waste. Clean (Weinh) 44:55–62

Santos RMMD, Gonçalves RGL, Constantino VRL, Santilli CV, Borges PD, Tronto J, Pinto FG (2017) Adsorption of acid yellow 42 dye on calcined layered double hydroxide: effect of time, concentration, pH and temperature. Appl Clay Sci 140:132–139

Sen TK, Afroze S, Ang HM (2011) Equilibrium, kinetics and mechanism of removal of methylene blue from aqueous solution by adsorption onto pine cone biomass of Pinus radiata. Water Air Soil Pollut 218:499–515

Singh JS (2013) Anticipated effects of climate change on methanotrophic methane oxidation. Clim Change Environ Sustain 1(1):20–24

Singh JS (2014) Cyanobacteria: a vital bio-agent in eco-restoration of degraded lands and sustainable agriculture. Clim Change Environ Sustain 2:133–137

Singh JS (2015) Biodiversity: current perspective. Clim Change Environ Sustain 3(1):71–72

Singh JS (2016) Microbes play major roles in ecosystem services. Clim Change Environ Sustain 3:163–167

Singh JS (ed) (2019) New and future developments in microbial biotechnology and bioengineering: microbes in soil, crop and environmental sustainability. Elsevier, Amsterdam

Singh JS, Boudh S (2016) Climate change resilient crops to sustain Indian agriculture. Clim Change Environ Sustain 5:97–110

Singh JS, Singh DP (eds) (2019) New and future developments in microbial biotechnology and bioengineering: microbial biotechnology in agro-environmental sustainability. Elsevier, Amsterdam

Singh DK, Srivastava B (2001) Basic dyes removal from wastewater by adsorption on rice husk carbon. Ind J Chem Technol 8:133–139

Singh C, Tiwari S, Boudh S, Singh JS (2017a) Biochar application in management of paddy crop production and methane mitigation. In: Singh JS, Seneviratne G (eds) Agro-environmental sustainability: Vol (2) managing environmental pollution. Springer, Cham, pp 123–145

Singh JS, Koushal S, Kumar A, Vimal SR, Gupta VK (2017b) Book review: microbial inoculants in sustainable agricultural productivity- Vol. II: Functional application. Front Microbiol 7:2015

Singh JS, Kumar A, Singh M (2019a) Cyanobacteria: a sustainable and commercial bioresource in production of bio-fertilizer and bio-fuel from waste waters. Environ Sustain Indic 3-4:100008

Singh MK, Rai PK, Rai A, Singh S, Singh JS (2019b) Poly-β-hydroxybutyrate production by the cyanobacterium Scytonema geitleri Bharadwaja under varying environmental conditions. Biomol Ther 9(198):1–10

Sophia AC, Lima EC (2018) Removal of emerging contaminants from the environment by adsorption. Ecotoxicol Environ Saf 150:1–17

Thines KR, Abdullah EC, Mubarak NM, Ruthiraan M (2017) Synthesis of magnetic biochar from agricultural waste biomass to enhancing route for waste water and polymer application: a review. Renew Sustain Energy Rev 67:257–276

Tiwari AP, Singh JS (2017) Plant growth promoting rhizospheric *Pseudomonas aeruginosa* strain inhibits seed germination in *Triticum aestivum* (L) and *Zea mays* (L). Microbiol Res 8(7233):73–79

Vikrant K, Giri BS, Raza N, Roy K, Kim KH, Rai BN, Singh RS (2018) Recent advancements in bioremediation of dye: current status and challenges. Bioresour Technol 253:355–367

Vimal SR, Singh JS (2019) Salt tolerant PGPR and FYM application in saline soil Paddy agriculture sustainability. Clim Change Environ Sustain 7(1):23–33

Vimal SR, Gupta J, Singh JS (2018) Effect of salt tolerant Bacillus sp. and *Pseudomonas* sp. on wheat (*Triticum aestivum* L.) growth under soil salinity: a comparative study. Microbiol Res 9(1):1–14

Yu J, Zhang X, Wang D, Li P (2018) Adsorption of methyl orange dye onto biochar adsorbent prepared from chicken manure. Water Sci Technol 77(5-6):1303–1312

Zazycki MA, Godinho M, Perondi D, Foletto EL, Collazzo GC, Dotto GL (2018) New biochar from pecan nutshells as an alternative adsorbent for removing reactive red 141 from aqueous solutions. J Clean Prod 171:57–65

Zhang Z, Moghaddam L, O'Hara IM, Doherty WOS (2011) Congo red adsorption by ball-milled sugarcane bagasse. Chem Eng J 178:122–128

Zhang B, Dong Z, Sun D, Wu T, Li Y (2017) Enhanced adsorption capacity of dyes by surfactant-modified layered double hydroxides from aqueous solution. J Indust Eng Chem 49:208–218

Zhang J, Yan X, Hu M, Hu X, Zhou M (2018) Adsorption of Congo red from aqueous solution using ZnO-modified SiO2 nanospheres with rough surfaces. J Mol Liquids 249:772–778

Zhao G, Li C, Wu X, Yu J, Jiang X, Hu W, Jiao F (2018) Reduced graphene oxide modified NiFe-calcinated layered double hydroxides for enhanced photocatalytic removal of methylene blue. Appl Surf Sci 434:251–259

Zulfikar MA, Setiyanto H, Rusnadi Solakhudin L (2015) Rubber seeds (Hevea brasiliensis): an adsorbent for adsorption of Congo red from aqueous solution. Desalin Water Treat 56:2976–2987